THE NUCLEAR LIQUID–GAS PHASE TRANSITION IN THE LIGHT OF SYNERGETICS*

B. Zwieglinski[f]

for the ALADIN Collaboration:

[a]Gesellschaft für Schwerionenforschung, 64291 Darmstadt, Germany
[b]Dipartimento di Fisica, Universita di Milano and I.N.F.N., 20133 Milano, Italy
[c]Dipartimento di Fisica dell'Universita and I.N.F.N., 95129 Catania, Italy
[d]Institut für Kernphysik, Universität Frankfurt, 60486 Frankfurt, Germany
[e]Forschungszentrum Rossendorf, 1314 Dresden, Germany
[f]A. Soltan Institute for Nuclear Studies, Hoża 69, 00-681 Warsaw, Poland
[g]H. Niewodniczanski Institute of Nuclear Physics, 31-342 Cracow, Poland
[h]NSCL, Michigan State University, East Lansing, MI-48824, USA

(Received December 17, 2001)

The nuclear liquid–gas phase transition is treated as the phenomenon of spontaneous symmetry breaking. A quasistationary state is formed at the end of nucleon–nucleon cascade in the residue, possessing the spherical symmetry, same as the projectile and target had in their ground states. This symmetry is broken in the course of fragment formation stage, at the end of which emerges a multi-cluster configuration. The nuclear liquid–gas phase transition is thus inscribed onto the list of critical phenomena considered by synergetics.

PACS numbers: 25.70.Pq

1. Introduction

The collision of two relativistic heavy ions at peripheral to semicentral impact parameters is a destructive process leading to the breakdown of the former order (*i.e.* the shell-model structure of each of the colliding partners), which is followed by a self-organization of matter, resulting in the cluster structure of the residues. This cluster structure is further reflected in the pattern of the detected Intermediate Mass Fragments (IMFs) following the residue breakup. The notion of self-organization was introduced into multi-fragmentation by Bondorf *et al.* in a seminal paper [1] without an explicit reference to synergetics, where it plays the central role.

* Presented at the XXVII Mazurian Lakes School of Physics, Krzyże, Poland, September 2–9, 2001.

Synergetics is a part of nonlinear science dealing with self-organization in non-equilibrium systems, characterized by the appearance of *dissipative structures* through the amplification of appropriate fluctuations [2]. Its field of investigation encompasses a wide range of problems from physics, chemistry and biology whose solutions are nonlinear functions of the variables involved. In applications to physics problems a starting point is identification of the solution corresponding to equilibrium conditions, which is called the *thermodynamic branch*. When the system is driven away from equilibrium, nonlinearities start to dominate, eventually causing instability of the thermodynamic branch at some critical value of the external constraints. It may then make a transition (*bifurcation*) onto a different solution called *dissipative branch*. The new state that emerges following the bifurcation often has a spatial and/or a temporal order. An illustrative example for the emergence of a dissipative structure is offered by a layer of fluid contained between two transparent parallel plates, which is heated from below and viewed from the top [3]. The system in question is described by thermo-hydrodynamic equations. When the temperature difference between the plates $\Delta T = T_2 - T_1$ is small, heat is conducted by diffusion, which is spatially homogeneous. However, when the temperature gradient is increased beyond a critical value this mode becomes unstable, giving way to a convective mode visible by the appearance in the fluid of a regular pattern of hexagonal Rayleigh–Bénard convection cells. The translational symmetry in the plane of the cell is broken as the result of this phase transition. Another example of critical behavior is offered by a laser cell, occurring when the pumping light intensity exceeds the threshold for the lasing action. The latter corresponds by its characteristics to a second order equilibrium phase transition in macrosystems [4].

The examples cited above refer to stationary nonequilibrium phase transitions. Light fragment formation in the initial stages of heavy ion interaction bears qualitative similarity to the mechanism of pattern formation in the first of the above two examples. However, the external directed heat flux in the colliding nuclear species is a transient of a short duration. The caloric curve measured by the ALADIN Collaboration [5] indicates that the nuclear liquid–gas phase transition is first order. In studies of first-order phase transitions in classical liquids [6] a system is rapidly quenched from a one-phase, thermal equilibrium state to a one-phase, nonequilibrium state inside its coexistence line. This quenched system then gradually evolves from this nonequilibrium state to an equilibrium thermodynamic state which consists of the coexisting phases of a liquid and a gas. It does so by the temporal development of spacial fluctuations which take the initialy homogeneous system through a sequence of inhomogeneous states which are far from

equilibrium. This dynamical evolution is highly nonlinear. It can be considered as a limiting case, with vanishing external fluxes, of pattern formation scenarios illustrated with the above two examples.

The aim of the present work is to present and discuss experimental evidence in favor of the occurrence of an analogous nonequilibrium transition state in the residue evolution. In Sec. 2 we present a chronogram for a relativistic heavy ion collision leading to multi-fragmentation of the residues. A transition from the one-phase, nonequilibrium state of the nuclear Fermi liquid to the equilibrium state of the interacting nucleons and clusters occurres in the *fragment formation* stage of the residue evolution. Sec. 3 is devoted to a discussion of the experimental evidence supporting this suggestion. In Sec. 4 we address the complementary points of view on dynamics of phase separation in the liquid–gas coexistence region of the nuclear phase diagram. We quote the results of Boltzmann–Langevin calculations to provide orientation as to different quantities related to spinodal decomposition, in particular on duration of the latter stage. In Sec. 5 we conclude.

2. Chronogram of the residue evolution

Relativistic heavy ion collisions serve as a unique tool to study thermodynamical properties of finite nuclear systems in a wide range of excitation energy, beginning below the multi-fragmentation threshold in peripheral collisions and ending above the complete disassembly close to central ones. The systems in question are residues (or spectators) of the projectile and target. We will consider collisions of a symmetric $A_p + A_t (A_p = A_t \equiv A_i)$ system, which justifies an assumption that, on average, the residues of the colliding partners evolve in the same way in time. One can roughly divide history of the collision, which terminates with multi-fragmentation, into four stages with the following tentative durations:

(i) Contact or fireball stage ($\tau_{\rm ct} \approx 15$–20 fm/c, the time of free passage of the Lorentz-contracted collision partners).

(ii) Pre-equilibrium emission ($\tau_{\rm eq} \approx 40$–75 fm/c).

(iii) Fragment formation ($\tau_{\rm Ff} \leq 300$ fm/c; excitation energy dependent).

(iv) Coulomb explosion ($\tau_{\rm Coul} \simeq 50$ fm/c).

The lengths of the last three stages add up to the total residue lifetime, $\tau_{\rm res} = \tau_{\rm eq} + \tau_{\rm Ff} + \tau_{\rm Coul}$. Two such histories are depicted as event chronograms in Fig. 1. The initial and final instants for the stages *(i)–(iv)* are labeled with the consecutive integers from 0 to 4 in Fig. 1(a).

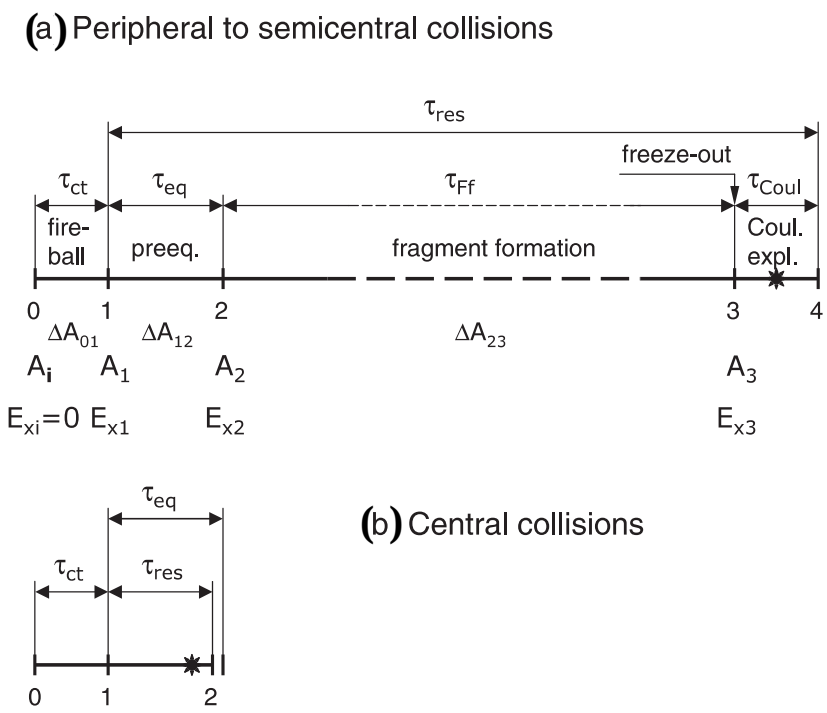

Fig. 1. Chronograms of two multi-fragmentation events are shown schematically for different collision centralities. It is assumed that the equilibration time, $\tau_{\rm eq}$, is independent of the initial excitation energies, E_{x1}, reached at the different impact parameters. The meaning of other symbols is explained in the text.

The fireball acts as a source of the initial excitation energy for the residues. Violent nucleon–nucleon collisions occurring in the overlap zone displace nucleons of the projectile (target) from the occupied states below the Fermi level into the fireball and onto the unoccupied states above the Fermi level. As a consequence, the residue enters the consecutive stage *(ii)* with mass, A_1, reduced by, ΔA_{01}, relative to the projectile $A_1 = A_i - \Delta A_{01}$, and excitation energy, E_{x1}, stored in multiparticle–multihole excitations. Both ΔA_{01} and E_{x1} are increasing functions of the overlap volume, which increases with the increasing collision centrality. After the residues have separated in space from the fireball (instant 1) they relax independently towards equilibrium via an internal cascade, mediated by nucleon–nucleon collisions. The residue is left in a state of (quasi)equilibrium as it enters stage *(iii)* (at the instant 2) with mass, $A_2 = A_1 - \Delta A_{12}$, and excitation energy, E_{x2}. Pre-equilibrium nucleons are responsible for the removal of most of ΔA_{12} and the initial excitation energy, E_{x1}. However, a fraction of these is carried away also by light charged composites with $Z \leq 2$, which are

formed by a successive coalescence of the cascading nucleons. The residue's internal structure reorganizes during the time of fragment formation, τ_{Ff}, from the initial single-center multi-exciton state into the multi-center freeze-out configuration. Evaporation of nucleons, α-particles and γ-rays proceeds throughout this stage, so that at freeze-out (instant 3) its mass decreased down to, $A_3 = A_2 - \Delta A_{23}$, and excitation energy down to, E_{x3}. The loss of neutrons tends to lower their multi-fragmentation barriers, therefore, the independently evolving systems explode (instant 4) on a short time scale, τ_{Coul}, treated as the stage (*iv*) in the above scheme. The time scale $\tau_{\mathrm{Coul}} \approx 50$ fm/c, quoted above, was determined by the ISiS Collaboration in the IMF–IMF relative velocity correlation measurements [7]. Masses and kinetic energies of the individually resolved products of the residue disassembly are used to reconstruct $\langle E_{x3}\rangle/\langle A_3\rangle$, while double yield ratios of light particles and/or IMFs serve to determine its temperature, T_3, at freeze-out. A functional dependence of T_3 on $\langle E_{x3}\rangle/\langle A_3\rangle$ is the caloric curve.

In Fig. 2 we present the average residue mass $\langle A_3\rangle$, charge $\langle Z_3\rangle$ and excitation energy per nucleon $\langle E_{x3}\rangle/\langle A_3\rangle$ at freeze-out as functions of the collision centrality for ^{197}Au+^{197}Au collisions at 600 MeV/nucleon. The latter excitation energies were used to construct the caloric curve of Ref. [5]. The range of excitation energies within which the residue lifetime, τ_{res}, exceeds the equilibration time, τ_{eq}, the situation depicted in Fig. 1(a), extends from the multi-fragmentation threshold at ≈ 2 MeV/nucleon up to ≈ 10 MeV/nucleon. This covers the liquid-gas coexistence region, corresponding to the plateau of the caloric curve. In Fig. 1(b) the lifetime became shorter than the equilibration time, because excitation energies are reached at which the system is so diluted that the attractive inter-nucleon forces are no longer capable to bind it together long enough. This situation starts to prevail above the vaporization threshold, indicated as the initial point of the linear rise of the gas branch of the caloric curve. This occurres for the impact parameters corresponding to $20 \leq Z_{\mathrm{bound}} \leq 30$. The residue in question is close to a Mo nucleus, with the mean excitation energy ≈ 12 MeV/nucleon. Taking into account these remarks, it would be more appropriate to associate with the stage *(ii)* a more general term, *pre-breakup emission*, which does not presume termination of the residue evolution in the state of (quasi)equilibrium.

The term *chronogram* was introduced in the work of Durand *et al.* [8], in which the authors refer to time scales encountered in heavy ion collisions in the Fermi energy domain. It should be stressed, however, that in the latter collisions the deposition of initial excitation energy, E_{x1}, is less precisely defined in time than in the relativistic domain, having as an unavoidable consequence an exchange of nucleons (cross-talk) and excitation energy loss prior to a separation of the residues.

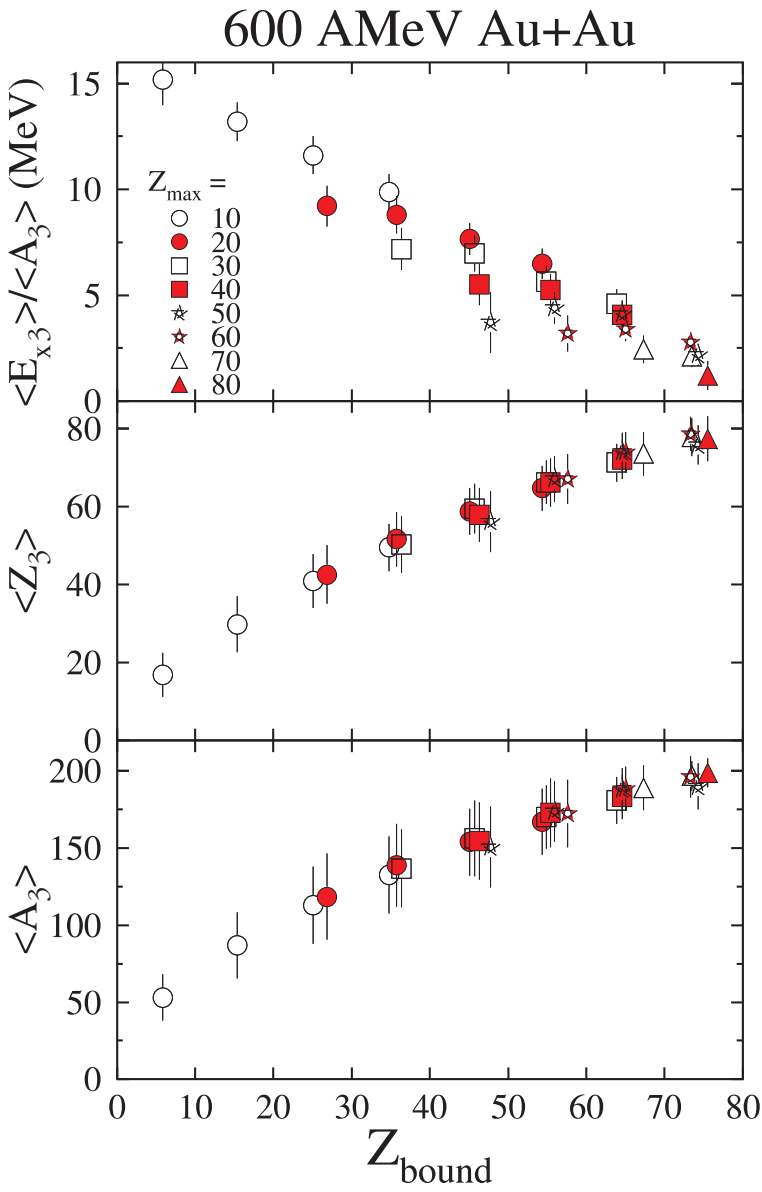

Fig. 2. Average residue mass $\langle A_3 \rangle$, charge $\langle Z_3 \rangle$ and excitation energy per nucleon $\langle E_{x3} \rangle / \langle A_3 \rangle$ as functions of Z_{bound} and for several gates on the largest observed charge Z_{max}.

In Sec. 3 we discuss features of experimental data which provide evidence on the occurrence of a quasistationary fragment formation stage *(iii)* in the residue evolution.

3. Experimental evidence on the fragment formation stage

It is clear from the preceding section that particles with different A, Z carry a different message about the system evolution. For example, nucleons and α-particles are expected to be emitted throughout the entire history, whereas IMFs only in the final stage *(iv)*. We define IMFs as fragments with $3 \leq Z \leq 30$, with the upper limit in Z imposed to eliminate from consideration fission fragments. The emitted particles have different kinematical properties in the laboratory system, depending on rapidity of the reference frame and transverse momentum acquired in the interaction, which makes it necessary to resort for their detection to different techniques. We will refer in the foregoing mostly to the ALADIN Collaboration results for ^{197}Au+^{197}Au at 1 GeV/nucleon [9–11] with a short détour to γ-rays measured by the TAPS Collaboration at the end of Sec. 3.1.

Products of multi-fragmentation in the stage *(iv)* are emitted isotropically in the remnant frame with velocities defined by decay energy. Particles from the projectile residue proceed in the laboratory within a narrow cone in the forward direction at these relativistic energies (*kinematical focusing*). The charged ones can, therefore, be detected with a high efficiency with a device possessing a small entrance aperture, such as the ALADIN magnetic spectrometer [12]. This method of detection was used to study IMFs (see Sec. 3.2) in the projectile fragmentation experiment S114 [9]. However, ALADIN's threshold for particle identification was at Z=2. Moreover, it has intrinsically low efficiency for the stage *(i)* and *(ii)* Z=1 particles, because of large transverse momenta playing role in these stages. The complementary information on light particles, including hydrogen isotopes, was obtained in the experiment S117 [10,11], in which particle spectra were measured from the target residue, slowly recoiling in the lab. In both experiments impact parameter involved in the collision was determined using $Z_{\rm bound}$ value of the fragmentation products measured event-wise with the ALADIN forward spectrometer. $Z_{\rm bound}$ is defined as a sum, $Z_{\rm bound}=\Sigma_i Z_i$, where the summation goes over fragments with $Z_i \geq 2$ for the given event.

3.1. Light particles and γ-rays

The spectra of light charged particles used to draw the conclusions presented below were measured with the aid of a four-element high resolution telescope set at the polar angle $\theta_{\rm lab} = 150^\circ$ relative to the direction of incidence of 1 GeV/nucleon ^{197}Au beam from the SIS18 synchrotron at GSI [11]. The spectra of neutrons were studied with the neutron detector LAND [10]. Fig. 3 is a summary of their main characteristics, which are displayed as functions of $Z_{\rm bound}$. Collision centrality is inversely correlated with the $Z_{\rm bound}$ value.

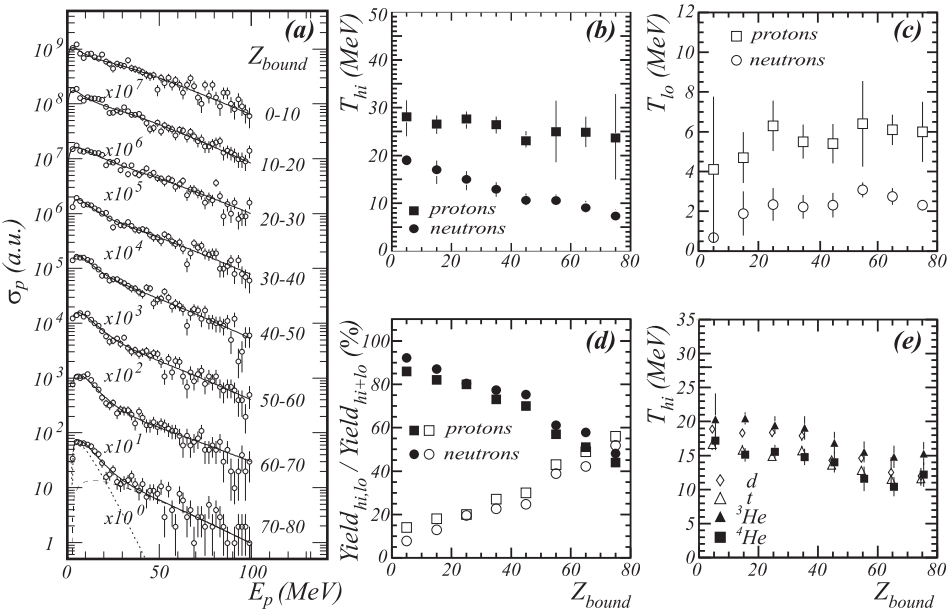

Fig. 3. Summary of the main characteristics of light particle spectra measured at $\theta_{\rm lab}$=150° in ^{197}Au+^{197}Au collisions at the projectile energy of 1 GeV/nucleon; (a) energy spectra of protons for different $Z_{\rm bound}$ bins and the results of two-component Maxwell–Boltzmann fits (solid lines). The fitted low- (lo, dotted line) and high-temperature (hi, dashed line) components are indicated for the spectrum labeled $Z_{\rm bound}$=70–80; (b), (c) temperatures extracted from the fits to nucleon spectra. (d) Relative contributions of the high- (closed symbols) and low-temperature (open symbols) components to nucleon spectra; (e) Temperatures resulting from the fits to experimental spectra for light composites as functions of $Z_{\rm bound}$.

A salient feature of the nucleon spectra are two components with different slopes, most pronounced in peripheral collisions, corresponding to $Z_{\rm bound}$ ranges 70–80 and 60–70 in Fig. 3(a). Following this observation all spectra were fitted with a sum of two Maxwell–Boltzmann distributions with different slopes, typified by the inverse-slope parameters, $T_{\rm hi,lo}$. An additional parameter in the case of charged products was the Coulomb correction, $V_{\rm c}$, assumed equal for the two spectrum components. The low temperature component, $\sigma_{\rm lo}$, is marked with the dotted line, while the high temperature one, $\sigma_{\rm hi}$, with the dashed line for the spectrum labeled $70 \leq Z_{\rm bound} \leq 80$. Solid lines represent their sum for this and the remaining $Z_{\rm bound}$ bins in Fig. 3(a). The Coulomb interaction effect is parametrized in such a way that the Maxwell–Boltzmann cross sections vanish below $V_{\rm c}$. A similar procedure was followed with regard to neutron spectra taken with the neutron spectrometer LAND. Figs. 3(b) and 3(c) display the fitted temperatures,

$T_{\rm hi}$ and $T_{\rm lo}$, respectively, for nucleons in the entire impact parameter range. A summary of the relative integrated yields, $Y_{\rm hi,lo}/Y_{\rm hi+lo}$, as functions of $Z_{\rm bound}$, is displayed in Fig. 3(d).

The slope parameters $T_{\rm lo}$, presented in Fig. 3(c), are of the order of a few MeV, such as typical evaporative values. This indicates that the components $\sigma_{\rm lo}(E_{p,n})$ are emitted in the stage *(iii)* from a hot quasistationary target remnant. The observed difference between $T_{\rm lo}$'s for protons and neutrons we ascribe to Coulomb effects. On the other hand, we tend to associate the components $\sigma_{\rm hi}(E_{p,n})$ with emissions within the pre-equilibrium stage *(iii)*. A similar two-component structure of the measured α-spectra [11] (not shown) with the low temperatures $T_{\rm lo} \approx 4$–$5\,$MeV is a further evidence for the occurrence of the quasistationary, evaporative stage *(iii)* in the residue evolution.

The relative contribution of the low-temperature component $Y_{\rm lo}/Y_{\rm hi+lo}$ (Fig. 3(d), open symbols) decreases rapidly with decreasing $Z_{\rm bound}$, to become hardly discernible in the experimental spectra with $Z_{\rm bound} \leq 30$. The average mass number $\langle A_3 \rangle$ of a residue with which one deals for $Z_{\rm bound} \leq 10$ is about 40 and the average excitation energy per nucleon therein $\langle E_{x3} \rangle / \langle A_3 \rangle \approx 24\,$MeV/nucleon [11, 17]. The magnitude of the fitted ratio $Y_{\rm lo}/Y_{\rm hi+lo}$ at these low $Z_{\rm bound}$ values, where the signature of evaporative events gradually disappears (see Fig. 3(a)), critically depends on the assumed shape of $\sigma_{\rm hi}(E_p)$ at low E_p. We have performed BUU calculations using the program BUU255 of Danielewicz [13], which describes the initial stages *(i)* and *(ii)* of the projectile-target interaction, in order to obtain a realistic estimate of this shape at low nucleon energies. Fig. 4 presents the proton spectrum (closed dots) calculated in the impact parameter range corresponding to $Z_{\rm bound} \leq 10$. The Coulomb hole at low proton energies in the BUU spectrum (Fig. 4, solid line) is shallower than that displayed by the Maxwell–Boltzmann formula for $\sigma_{\rm hi}(E_p)$ with the barrier height $V_{\rm c} \approx 4$ MeV assumed for all $Z_{\rm bound}$ bins in Fig. 3(a) and plotted as the dashed line for $70 \leq Z_{\rm bound} \leq 80$. The estimate given by BUU thus leaves less room for $\sigma_{\rm lo}(E_p)$ at low E_ps, indicating that the open squares in the range of $Z_{\rm bound} \leq 20$ in Fig. 3(d) are rather upper bounds for the relative contribution of this component. A disappearance of the evaporative component from the proton spectra may indicate, therefore, that the residue lifetime becomes too short to reach thermalization after exceeding by its excitation energy some limiting value. This limiting value is in fact the vaporization threshold in the residue. The multi-fragmentation barrier disappears above this threshold, as we have already stressed in Sec. 2. In summary, the $Z_{\rm bound}$ dependence of relative yields of the soft component of nucleon spectra, manifested in Fig. 3(d), serves as a basis for our hypothesis of excitation energy dependent time of fragment formation, $\tau_{\rm Ff}$. This is schematically expressed in Figs. 1(a) and 1(b).

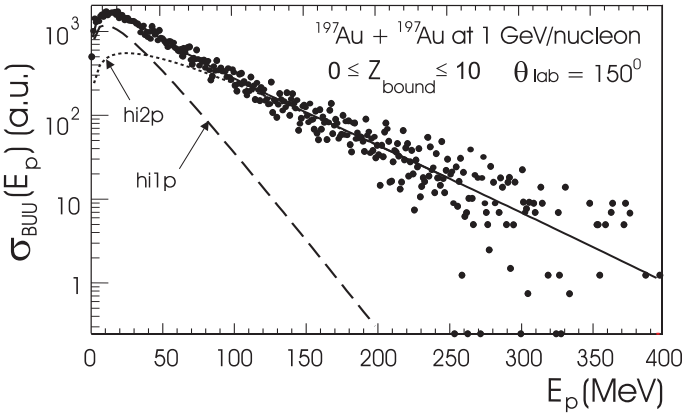

Fig. 4. Energy spectrum of protons emitted in near central collisions into $\theta_{\rm lab} = 150^\circ$ as predicted by BUU255 (filled circles). Dotted line (hi2p) indicates the component emitted directly from the fireball [stage *(i)*], while the dashed line (hi1p) the pre-equilibrium one [stage *(ii)*]. Solid line is the sum of these two contributions.

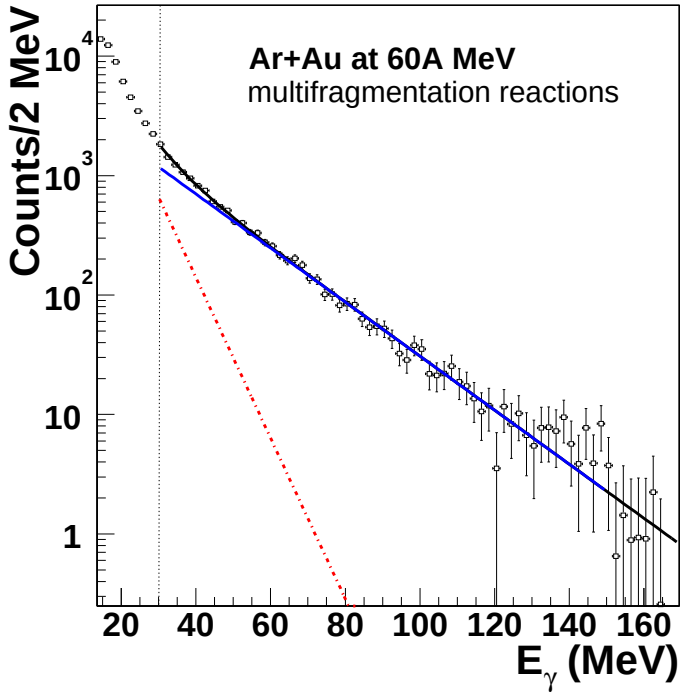

Fig. 5. Hard photon spectrum measured in the NN center-of-mass for multi-fragmentation collisions of the system ^{36}Ar+^{197}Au at 60 MeV/nucleon [16]. The spectrum has been fitted with a sum of two exponential distributions, a direct (solid line) and a thermal one (dash-and-dot line).

The presence of fast and slow stages of the residue evolution has been established nearly simultaneously by the EOS [14] and the ALADIN [15] Collaborations based on the features observed in proton spectra. Recently, this conclusion has been confirmed in a study of hard γ-rays emitted in ^{36}Ar+^{197}Au collisions at 60 MeV/nucleon [16] with the electromagnetic spectrometer TAPS. The measured γ-ray spectra were tagged with light charged particles and IMFs detected with the aid of two multi-detector arrays. Fig. 5 displays the spectrum measured in events characterized as multi-fragmentation by the associated particle yields. The spectrum is a superposition of two exponential contributions with the slope parameters $E_d = 20.2 \pm 1.3$ MeV and $E_t = 6.0 \pm 0.8$ MeV, whose origin was uniquely assigned to the pre-equilibrium and the thermal emission, respectively. The latter slope is remarkably close to our equilibrium proton temperatures, $T_{\rm lo}$, for mid-central collisions ($Z_{\rm bound} \approx 30 \div 50$) in Fig. 3(c). It is gratifying to note that our conclusions are supported by the perturbative probes.

In the next subsection we examine the evidence provided by IMFs emitted in projectile fragmentation.

3.2. Intermediate mass fragments (IMFs)

Fig. 6 presents rapidity spectra for fragments with $Z = 2 \div 5$ emitted in ^{197}Au+^{197}Au collisions at 1 GeV/nucleon, measured with the ALADIN forward spectrometer. The downward shift of the solid line relative to the dashed one indicates that projectile residues emerge from the fireball stage *(i)* with reduced rapidity due to nucleon abrasion and scattering suffered in the course of this stage. One notes differences between shapes of the spectra with $Z \leq 4$ and $Z \geq 5$. A peak, close to the perfect Gaussian, centered on the solid line, is a notable feature of the spectrum for $Z = 5$ and those for the higher Z values (not shown) [9]. The spectra with $Z \leq 4$ reveal also tails extending towards lower rapidities. Their relative contribution is progressively increasing with decreasing Z. Inspection of the same spectra in the transverse momentum ($p_{\rm T}$)-rapidity plane demonstrates that the tails extend further away in $p_{\rm T}$ from the y-axis than the Gaussian part. One may conclude, therefore, that IMFs contributing to the background underlying the peaks are of dynamical origin and are produced in the pre-equilibrium stage *(ii)*. On the other hand, those constituting the peaks are emitted from the equilibrated remnants in the stage *(iv)*. The dynamical process in question, engaged in the stage *(ii)*, is most probably coalescence of the consecutive nucleons. Besides the above mentioned smooth Z-dependence one notes also the tendency of increasing tail contribution with the increasing bombarding energy (see [9]).

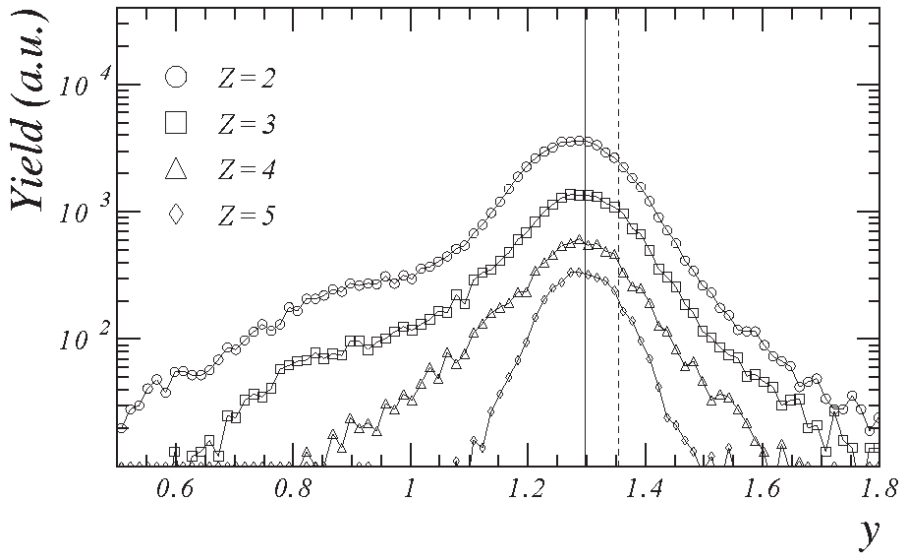

Fig. 6. Rapidity spectra of fragments with $Z = 2 \div 5$ measured with the ALADIN time-of-flight wall in ^{197}Au+^{197}Au collisions at 1 GeV/nucleon. The vertical solid line indicates the position of peak centroids, the dashed one marks the projectile rapidity.

The perfect Gaussian shape of the rapidity distributions for IMFs with $Z \geq 5$ gives a complementary evidence, that the system freeze-out is preceded by the fragment formation stage *(iii)*, which effectively isolates it from the preceding stages of turbulent evolution.

4. Pattern formation in the nuclear liquid–gas phase transition

At the end of the second stage *(ii)* the residue appears quenched below the liquid–gas coexistence line into the metastable binodal or unstable spinodal region of the nuclear phase diagram. At this instant the system is still homogeneous and preserves the original single-center spherical symmetry, the projectile and target have had in their ground states. This is because only the single-particle degrees of freedom were engaged in the nucleon–nucleon cascade. This symmetry will be broken in the course of the consecutive evolution of the system towards the true equilibrium, which corresponds to separated phases of liquid and gas.

From the metastable region the phase transition proceeds by nucleation, while from the unstable one by spinodal decomposition [6]. Both these modes are triggered by density fluctuations, which form small droplets of

a new phase. In the metastable region the energetically unfavorable process of creation of a surface of new phase has the result that when a droplet is below a certain threshold size (*critical droplet*) it is unstable and disappears again. Nucleation consists in production of supercritical droplets by fluctuations, which then spontaneously grow to generate the new phase. When the droplets are produced in small numbers, the reactions between clusters and single vapor nucleons provide the mechanism for growth of clusters. The rates for formation from the supersaturated phase to the droplet phase is governed by "potential barriers" in the Gibbs free energy per particle. The droplet model of Fisher, considered by Moretto and collaborators [18], has elements in common with this scenario.

On the other hand, even infinitesimal density fluctuations are sufficient to initiate decomposition in the mechanically unstable spinodal region, provided they exceed a critical wavelength λ_c [6]. For infinite nuclear matter the most unstable wavelength is near $\lambda \approx 10$ fm. A study of spinodal instabilities in finite nuclei along this line has been initiated by Randrup *et al.* [19] and later advanced in a series of papers by the GANIL theory group (see *e.g.* [20]) within the Boltzmann–Langevin approach. The Langevin term in the Boltzmann equation accounts for the fluctuating part of the collision integral. We will quote the results they obtained for the system of A=210 nucleons at half normal density and at temperature T=3 MeV [20], which will provide orientation as to different quantities related to spinodal decomposition in nuclei, in particular on $\tau_{\rm Ff}$. For this finite system instabilities are decomposed into eigen-modes with definite angular momenta. The most unstable L-values appear to be around L=5, corresponding to a surface wave characterized by a distance between adjacent maxima $\lambda \approx 2\pi R/L \approx 10$ fm. The initial growth of instabilities appears to be exponential with a characteristic growth time $\tau \approx 35$ fm/c. The fragments are formed in approximately 100 fm/c after the system has been initialized in the spinodal region, which corresponds to $2 \div 3\tau$. The dominance of L=5–6 leads to the formation of 5 to 6 almost equally sized fragments. The Z-values of the largest three, when plotted as events on a Dalitz diagram, populate mostly its central part. This pattern is qualitatively similar to the one observed by the ALADIN Collaboration in the early multi-fragmentation studies of the system ^{197}Au+^{197}Au at 600 MeV/nucleon [21]. For this reason, this model and its ancestor, dubbed Brownian One Body (BOB) dynamics [20], which predicts somewhat longer $\tau_{\rm Ff} \approx 150$ fm/c, deserve a more detailed quantitative confrontation with data obtained in peripheral to semicentral relativistic heavy ion collisions. Moreover, its point of view on the system dynamical evolution as a continual branching under the influence of the fluctuating collision integral, is completely in the spirit of synergetics.

We do not possess similar time scale estimates for nucleation from the metastable region of the phase diagram. For classical liquids very long time scales are predicted and observed [6] in vicinity of the critical temperature (*critical slowing-down*). Away from the critical temperature it is fair to expect similar time scales in nucleation and spinodal decomposition. In the extreme peripheral collisions residues are left below the multi-fragmentation threshold of ≈ 2 MeV/nucleon in the domain of thermodynamic branches. In this domain evaporative processes follow the initial pre-equilibrium cascade. The first dynamical instability encountered at somewhat higher excitations is that of fission. A counterpart of the above $\tau_{\rm Ff}$ is the fission transient time, $\tau_{\rm D}$. The emission of pre-scission neutrons, charged particles and dipole γ-rays in different fissioning systems has been ascribed to finite $\tau_{\rm D} \approx 10^{-19}$ sec. Recent estimates based on the analysis of fission probabilities of neighboring isotopes in the mass region $A \approx$185 led to $\tau_{\rm D} \approx 10^{-20}$ sec [23].

5. Conclusions

We have considered multi-fragmentation in peripheral to semicentral ^{197}Au+^{197}Au collisions at 1 GeV/nucleon as an evolutionary process consisting of the four stages. The IMFs with $Z \geq 5$ do not carry "fingerprints" of the first two violent interaction stages. On the other hand, one finds manifestations of nucleon–nucleon interaction effects for $Z \leq 5$, progressively increasing with the decreasing particle Z-value. We tend to ascribe this fraction of the emitted light-composites d, ^{3}He, t and IMFs with $2 \leq Z \leq 5$ to a successive coalescence of a nucleon in the second internal cascade stage of the residue evolution. These contributions are easily discernible in the experimental spectra by their distinct momentum transfer dependence. However, the internal cascade stage lasts too short to cause multifragmentation. It comes to an end with the formation of a low-density quasistationary state posessing spherical symmetry. The soft components of nucleon, α-particle and γ-ray spectra are unambiguous signals that the system lives in a metastable state. Its lifetime is long enough, so that dynamical instabilities (presumably of the spinodal origin) develop, causing formation of clusters. The sudden loss of spherical symmetry and the missing binding, contributed by the last evaporated particle, provoke Coulomb explosion of the residue.

The role of interaction energy capable to bind the system long enough to allow the liquid–gas phase transition terminate is emphasized in this multifragmentation scenario. This condition is fulfilled for those combinations of residue masses, A_3, and their excitation energies, E_{x3}, which are encountered in the liquid–gas coexistence region of the caloric curve,

$2 \leq \langle E_{x3} \rangle / \langle A_3 \rangle \leq 10\,\mathrm{MeV/nucleon}$. Above the latter energy the signals of metastability disappear, indicating that the residue lifetime became shorter than the equilibration time. The residue entered the gas branch of the caloric curve.

This work was supported in part by the European Community under contract ERBFMGECT950083 and by the BMBF (Bonn) – KBN (the Polish State Committee for Scientific Research) (Warsaw) Collaborative Agreement in Science and Technology under contract POL-196-96. Illuminating and inspiring discussions with my colleagues from the ALADIN Collaboration are gratefully acknowledged. Moreover, I like to thank J.P. Bondorf, D.G. d'Enterria, H. Horiuchi and A. Mykulyak for providing me with graphics for the lecture and for this paper.

REFERENCES

[1] J.P. Bondorf, D. Idier, I.N. Mishustin, *Phys. Lett.* **B359**, 261 (1995).

[2] G. Nicolis, I. Prigogine, *Self-Organization in Nonequilibrium Systems, from Dissipative Structures to Order through Fluctuations*, Wiley, New York 1977.

[3] G. Venkataraman, V. Balakrishnan, *Synergetics and Dynamic Instabilities*, Procceidings of International School of Physics "Enrico Fermi", Course IC, Varenna, Italy, 24 June–4 July 1986, ed. G. Calioti and H. Haken, North-Holland, Amsterdam 1988, p. 175.

[4] H. Haken, *Synergetics, an Introduction, Nonequilibrium Phase Transitions and Self-Organization in Physics, Chemistry and Biology*, 2nd ed., Springer, Berlin, Heidelberg, New York 1978.

[5] J. Pochodzalla *et al., Phys. Rev. Lett.* **75**, 1040 (1995); J. Pochodzalla, *Progr. Part. Nucl. Phys.* **39**, 443 (1997).

[6] S.W. Koch, *Dynamics of First-Order Phase Transitions in Equilibrium and Nonequilibrium Systems, Lecture Notes in Physics* **207**, ed. H. Araki, J. Ehlers, K. Hepp, R. Kippenhahn, H.A. Weidenmüller, J. Zittarz, Springer, Berlin, Heidelberg, New York 1984.

[7] L. Beaulieu *et al., Phys. Rev. Lett.* **84**, 5971 (2000).

[8] D. Durand *et al., Phys. Lett.* **B345**, 397 (1995).

[9] A. Schüttauf *et al., Nucl. Phys.* **A607**, 457 (1996).

[10] C. Gross, PhD Thesis, Universität Frankfurt, GSI-Report DISS **98-21**, November, 1998.

[11] T. Odeh, PhD Thesis, Universität Frankfurt, GSI-Report DISS **99-15**, August, 1999.

[12] The ALADIN Collaboration, GSI-Report **88-08**, March, 1988.

[13] P. Danielewicz, Q. Pan, *Phys. Rev.* **C46**, 2002 (1992); P. Danielewicz, *Phys. Rev.* **C51**, 716 (1995).

[14] J.A. Hauger *et al., Phys. Rev. Lett.* **77**, 235 (1996); J.A. Hauger *et al., Phys. Rev.* **C57**, 764 (1998); J.A. Hauger *et al., Phys. Rev.* **C62**, 024616 (2000).

[15] Hongfei Xi *et al., Z. Phys.* **A359**, 397 (1997).

[16] D.G. d'Enterria *et al., Phys. Rev. Lett.* **87**, 022701 (2001); D.G. d'Enterria, PhD Thesis, Université de Caen and Universitat Autonoma de Barcelona, *Report GANIL T* **00 03**, 2000.

[17] U. Lynen *et al., Nucl. Phys.* **A630**, 176c (1998).

[18] L.G. Moretto *et al.*, Proc. of the XXXIX Int. Winter Meeting on Nuclear Physics, Bormio, Italy, 22 – 27 January 2001, ed. I. Iori and A. Moroni, "Ricerca Scientifica ed Educazione Permanente", Suppl. 117, 2001, p. 15; J.B. Elliott *et al., Phys. Rev. Lett.* (2001) submitted for publication.

[19] J. Randrup, B. Remaud, *Nucl. Phys.* **A514**, 339 (1990).

[20] A. Guarnera, M. Colonna, Ph. Chomaz, *Phys. Lett.* **B373**, 267 (1996).

[21] P. Kreutz *et al., Nucl. Phys.* **A556**, 672 (1993).

[22] A. Guarnera, M. Colonna, Ph. Chomaz, J. Randrup, *Phys. Lett.* **B403**, 191 (1997).

[23] K.X. Jing *et al., Phys. Lett.* **B518**, 221 (2001).